Nano-Structures & Nano-Objects 24 (2020) 100547

Contents lists available at ScienceDirect

Nano-Structures & Nano-Objects

journal homepage: www.elsevier.com/locate/nanoso

Direct laser-induced deposition of AgPt@C nanoparticles on 2D and 3D substrates for electrocatalytic glucose oxidation

Anna Vasileva [a,*], Sandra Haschke [b], Vladimir Mikhailovskii [c], Anastasia Gitlina [a,d], Julien Bachmann [a,b], Alina Manshina [a]

[a] Department of Chemistry Saint-Petersburg State University Ulyanovskaya 5, Saint-Petersburg 198504, Russian Federation
[b] Department of Chemistry and Pharmacy, Chemistry of Thin Film Materials Friedrich-Alexander University Erlangen-Nürnberg Cauerstraße 3, Erlangen 91058, Germany
[c] Interdisciplinary Resource Centre for Nanotechnology of Scientific Park Saint-Petersburg State University Ulyanovskaya 1, Saint-Peterburg 198504, Russian Federation
[d] Ecole polytechnique fédérale de Lausanne, Institut des sciences et ingénierie chimiques, CH-1015 Lausanne, Switzerland

ARTICLE INFO

Article history:
Received 27 May 2020
Received in revised form 29 July 2020
Accepted 15 August 2020

Keywords:
Laser-induced deposition
AgPt@C NPs
Nanoporous anodic aluminum oxide
Electrocatalysis
Glucose oxidation

ABSTRACT

We present a new approach for the preparation of electrocatalytically active carbonaceous coatings embedding bimetallic nanoparticles (NPs) - AgPt@C structures, on surfaces with 2D and 3D geometry such as glass covered with indium tin oxide (ITO) film and anodic aluminum oxide substrates, respectively. We provide extensive characterization of the deposited structures and demonstrate their performance towards the electrocatalytic glucose oxidation, one half-reaction of biofuel cells. We observe that a preliminary surface treatment of the porous alumina substrate is essential for a homogeneous laser-induced deposition of AgPt@C nanoparticles across the whole pore depth.

1. Introduction

Compact electrochemical devices based on glucose electrooxidation on microelectrodes [1–4] could have a wide range of applications from food industry (analysis of glucose content in juices) [5,6] to medicine (as power sources for implanted cardiac stimulators and as glucose sensors in the blood stream) [7–10]. One approach for maximizing current (and power) density at macroscopically compact electrodes relies on nanostructured surfaces, which increase the electrochemically active specific surface area. Nanoporous anodic aluminum oxide (AAO) provides an interesting template system for the creation of such electrodes by coating with electrocatalyst. Their geometry of parallel, cylindrical pores is advantageous in providing a high surface area in a compact volume while allowing for efficient transport to and from the surface, thereby optimizing the overall catalytic activity of system [11–13]. The most attractive feature of AAO as a model template system is the direct control of the geometric parameters (diameter and length of the pores, interpore distance) based on the preparative parameters (voltage and duration of anodization, electrolyte type, subsequent isotropic chemical etching) [14,15]. Preparative techniques for synthesis of AAO templates are widely studied: developed methods of synthesis from different quality aluminum [16], investigated factors influence on regularity ratio of pores [17], found the ways to fabricate submicrometer scale dimple arrays [18]. In this article we suggest a nanostructured system for catalysis of glucose electrooxidation based on highly ordered AAO templates covered by AgPt@C nanoparticles (NPs). The decoration of nanostructured AAO templates was realized by laser-induced deposition (LID), which allowed single step AgPt@C NPs synthesis directly onto the 3D surface. The deposited NPs consist of a carbonaceous phase embedding bimetal AgPt nanoinclusions. The choice of AgPt nanoparticles was determined by several factors. In the field of electrocatalysis the bimetallic nanoparticles demonstrate superiority over constituent metal NPs due to strong electronic coupling resulting in strong enhancement of catalytic activity [19–21]. The special interest in creation and investigation of AgPt nanoparticles is determined by their activity in various electrochemical reactions [22–25]. However the creation of electrodes combining high specific surface area and bimetal NPs is not easy and multistep process. The choice of AgPt NPs as electrocatalysts in our work was connected with demonstration of both — LID deposition of bimetal NPs AgPt, as well as decoration of 3D AAO structures. As functionality testing of glucose oxidation was chosen as having practical meaning.

Laser-induced deposition is a method developed in the field of laser chemistry for generating various types of nanostructured solids upon laser irradiation of a solution of appropriate supramolecular precursors. Laser chemistry methods include

* Corresponding author.
E-mail address: anvsilv@gmail.com (A. Vasileva).

https://doi.org/10.1016/j.nanoso.2020.100547
2352-507X/

photochemically- and thermally induced nano- and microstructure formation [26–29], metal nanoparticles generation with laser ablation [30–32], as well as the formation of nanostructures in glasses [33,34]. The structures obtained in laser-induced processes have been applied in surface-enhanced Raman spectroscopy (SERS) [35–38], photo- and electrocatalysis [39–42] and nanophotonics [43–45]. Laser chemistry allows the experimentalist to control the reaction conditions accurately in a confined volume. In particular, the LID method enables one to deposit metal nanoparticles embedded in a carbon matrix on substrates of various topologies: planar ones such as microscope cover glasses and conductive indium tin oxide (ITO) films, but also three-dimensional ones such as silicon nanowires and nanoporous anodic aluminum oxide (AAO) [41,46]. A critical advantage of LID over more traditional techniques (such as wet chemical impregnation, galvanic deposition, or atomic layer deposition) is its ability to generate in a single experimental procedure a complex composite layer containing both the electrical conductor (carbon) and the electrocatalysts (metal nanoparticles). The LID method is based on photo-excitation of the precursor molecule and its following decomposition [47]. Then the formation of nanostructures from the precursor components takes place on the surface of the substrate. An appealing feature of the approach is the use of continuous low-intensity laser irradiation, which guarantees that there is no destructive effect both on the synthesized nanostructures themselves and on the substrates on which they are formed. The last circumstance is of critical importance for application of LID approach for decoration of nanostructured substrates such as nanoporous AAO. Scheme 1a, b demonstrates the principle experimental scheme of laser-induced deposition process. The structure of the organometallic complex $Pt_2Ag_4(C_2Ph)_8$ used as the LID precursor in this work is presented in Scheme 1c .

The large specific surface area of the NPs maximizes their catalytic performance [48,49]. Furthermore, LID also gives access to bimetallic NPs, which may exhibit higher electrocatalytic performance than their monometallic counterparts [50].

In this paper, we explore the adequacy of LID-generated nanostructured electrodes towards glucose oxidation in sense of practical applications in medicine and food industry. Biological media are predominantly pH-neutral or mildly acidic whereas fruit juices are mainly mildly acidic. However the majority of published articles have been focused on glucose oxidation in alkaline conditions. That is why glucose oxidation reaction in mildly acidic media (pH = 4) was chosen in our study for the electrocatalysis of a bimetallic system AgPt@C. We characterize the AgPt@C deposit on planar substrates and demonstrate that the procedure can be generalized to 3D substrates. A homogeneous LID deposit along the whole length of the AAO pores, however, requires a preliminary surface treatment. Such optimized nanostructured electrodes subsequently provide a significant improvement of glucose oxidation activity with respect to their planar counterparts.

2. Materials and methods

2.1. Materials and reagents

Aluminum plates (99.99%), were obtained from SmartMembranes. The ITO sputter target with purity >99.99% and disc shape from Stanford Advanced Materials was used. Cover glass slips with 0.15 mm thickness and 24 mm x 24 mm size were purchased from Levenhuk (G100 cover slips). $CuCl_2$ (>98% wt%), H_3PO_4 (84% wt%) and HCl (38% wt%) were used without additional purification. For solutions preparation bidistilled water was used.

Target hexanuclear complex $Pt_2Ag_4(C_2Ph)_8$ was synthesized according to published procedure [51] from cis-$[Pt(DMSO)_2Cl_2]$, $AgNO_3$ and phenylacetylene in dark under N_2 atmosphere using Schlenk technique. Cis-$[Pt(DMSO)_2Cl_2]$ was prepared following to published procedure [52] and used as obtained without additional purification. All reagents were purchased from commercial suppliers (Sigma Aldrich, Alfa Aesar and Fluka) and used as received without additional purification. Dichloromethane, acetonitrile, triethylamine and phenylacetylene were purified and distilled following to the standard procedures [53].

2.2. Synthesis of $Pt_2Ag_4(C_2Ph)_8$ precursor

$AgNO_3$ (161 mg, 0.948 mmol) and phenylacetylene (97 mg, 0.948 mmol) were dissolved in dichloromethane/acetonitrile solvents mixture (1:1, v/v, 4 mL) and triethylamine (96 mg, 0.948 mmol) was added dropwise. White suspension was stirred for 30 min at room temperature. Then, a solution of cis-$[Pt(DMSO)_2Cl_2]$ (100 mg, 0.237 mmol) in dichloromethane (2 mL) was added and the reaction mixture turned dark. After 8 h of stirring at room temperature AgCl was filtered off through a pad of Celite in a Pasteur pipette. The pad was washed with dichloromethane. The resulting red solution was evaporated to a minimum volume. By addition of acetone excess a yellow precipitate (150 mg, 78% yield) was obtained.

2.3. Substrates preparation

As 2D substrates, cover slips coated with 200 nm ITO (indium tin oxide) were used, with a resistivity of 90 Ω/cm. The ITO film was obtained by HF sputter-coating in a Torr CRC 622 Sputter Coater (first 20 nm were spattered at the pressure 6.6×10^{-3} Torr, then subsequent 180 nm at the pressure 3×10^{-3} Torr).

As 3D substrates, nanoporous anodic aluminum oxide with an average pore diameter of 350 nm and pore length of 14 μm was used. The templates were prepared in a two-step anodization process [12]. Aluminum plates of 2 cm $\times$ 2 cm size were placed in beakers featuring adapted openings and pressed onto a thick copper plate serving as the electrical contact. First, electropolishing of samples in a solution of $HClO_4$ in ethanol (volume ratio 1:3) was carried out for 5 min under +20 V, whereas a silver mesh served as the cathode. After electropolishing, the beakers with aluminum plates were thoroughly washed with distilled water. Next, disordered aluminum oxide pores were obtained on the aluminum surface upon anodization under +195 V at 0 °C for 1 h in 0.5 wt% phosphoric acid, then for 23 h in 1% phosphoric acid. The layer of porous oxide obtained was removed with chromic acid (2% H_2CrO_4 in 20% H_3PO_4) at 45 °C for 23 h. The second anodization step leading to ordered membrane pores was performed under +195 V at 0 °C in 0.5 wt% phosphoric acid for 1 h and afterwards in 1.0 wt% phosphoric acid under +195 V for 6 h. The metallic aluminum substrate was subsequently removed with a solution of 0.7 M $CuCl_2$ in 10% HCl, the procedure takes 50 min. The aluminum oxide barrier layer was finally deleted by treatment of the samples with 10 wt% H_3PO_4 at 45 °C for 45 min.

A set of the AAO templates was chemically functionalized from the gas phase in an atomic layer deposition reactor GEMStar XT (Arrandiance). After 4 pulses of water at room temperature, $tH_2N(CH_2)_3Si(OEt)_3$ was pulsed four times while the chamber was held at 80 °C. For water the durations of pulse, exposure, and pumping were 0.2 s, 40 s, and 60 s correspondingly. For silane precursor the durations of pulse, exposure, and pumping were 2 s, 100 s, and 200 s correspondingly.

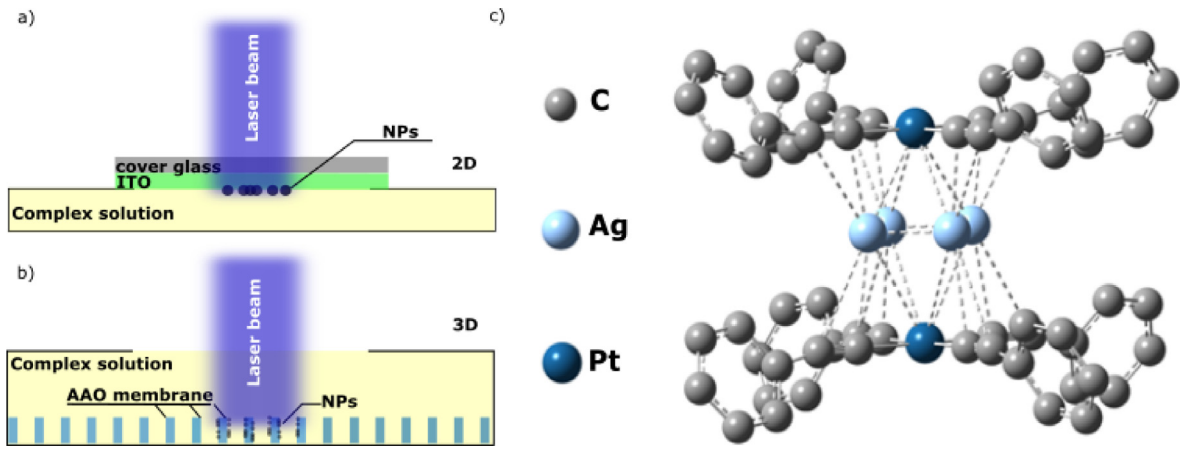

Scheme 1. Principles of laser-induced deposition: (**a**) scheme of laser-induced deposition on 2D substrates; (**b**) scheme of laser-induced deposition on 3D substrates; (**c**) structure of the organometallic $Pt_2Ag_4C_2Ph_8$ precursor used for LID.

2.4. Sample preparation by laser-induced deposition

A saturated (2.4 mM) solution of $Pt_2Ag_4C_2Ph_8$ organometallic precursor in acetophenone was prepared with 5 min of ultrasonication and subsequent 5 min of centrifugation at 10 000 rpm in a Sigma 2-16P (Sigma Laborzentrifugen). Then hydrazine was added to the solution in a molar ratio of 2:1 precursor to hydrazine. For the LID process, the prepared solution was either put into a glass cuvette (deposition on 2D substrates) or dropped onto the substrate (deposition on 3D substrates) and irradiated by the continuum wave CUBE laser source from Coherent (λ = 405 nm and a power density of 60 mW/cm^2). The laser beam was unfocused, sample was immobile relatively the laser beam, the exposure time was 20 min. These parameters allow obtaining the most homogeneous coverage of substrates with NPs without their agglomeration. The deposition area coincided with the laser beam diameter ca 2 mm. Finally, the samples were washed with acetone. For the current study we prepared one set of 2D samples (NPs on cover slips with ITO) and two sets of 3D samples (NPs on AAO as prepared and on AAO modified with silanization).

2.5. Sample characterization

The absorbance spectra were measured with a Precision Spectrophotometer Lambda 1050 UV/VIS/NIR. The precursor solution absorption spectra were recorded over the spectral range 370 nm–500 nm, while the absorption spectra of AgPt@C NPs deposited on ITO (2D samples) were determined in the range of 300 nm–450 nm with an integrating Ulbricht sphere. The substrate with NPs was placed in the sphere center. The morphology and composition of obtained samples were investigated by scanning electron microscopy (SEM) and energy dispersive X-ray analysis (EDX) with a scanning electron microscopes Zeiss Supra 40VP with Field Emission cathode, GEMINI electron-optics column, oil-free vacuum system, variable pressure (VP) operating mode, and with a JEOL JSM 6400 PC with LaB_6 cathode and silicon drift EDX detector from SAMx. The transmission electron microscope (TEM) images were obtained on a transmission electron microscope Zeiss Libra 200FE.

2.6. Electrocatalysis

For preparation of 2D electrodes, samples on ITO were glued to small copper plate (2 cm $\times$ 2 cm $\times$ 0.1 cm) with copper adhesive tape. For preparation of 3D electrodes, 800 nm ITO film was obtained by HF sputter-coating (first 20 nm were spattered at the pressure 6.6 $\times$ 10^{-3} Torr, then subsequent 780 nm at the pressure 3 $\times$ 10^{-3} Torr) onto one side of the sample based on nanoporous AAO in order to provide the electrical contact layer. The fact of completed formation of this contact layer was controlled by SEM. Then, the sample was glued to a copper plate with copper adhesive tape, with the ITO-covered side facing Cu. In both cases – 2D and 3D – Kapton polyamide non-conductive tape was used for masking and defining a circular opening of well-defined macroscopic size. It was laser-cut with a GCC LaserPro Spirit LS Laser to 2 cm $\times$ 2 cm pieces featuring a central circular hole of 1.5 mm diameter. Scheme 2 shows construction of electrodes.

The samples were investigated as the working electrode in a three-electrode electrochemical cell with Pt mesh as the counter-electrode and an Ag/AgCl (3 M KCl) reference electrode featuring a redox potential of +0.21 V versus NHE. All electrochemical data given in the paper are stated with respect to the Ag/AgCl reference. We performed glucose oxidation reaction in HCl at pH 4 in the absence and presence of 5 mM glucose. To confirm the presence of platinum in the system, the hydrogen evolution reaction (HER) was carried out. For HER, we used HCl at pH 4 as the electrolyte. The measurements were carried out at room temperature on potentiostats Gamry Interface 1000. Cyclic voltammetry was carried out starting at the open-circuit potential with 3 s time delay between OCP and CVA measurements, CVA was performed with a scan rate of 50 mV s^{-1}, three cycles were measured for each case without time delay between the cycles. The voltage range for hydrogen evolution reaction is from −0.7 V to 1.5 V. The voltage range for glucose electrooxidation is from −0.2 V to 0.5 V. For all listed cases, the third CV cycle is presented. The current density was calculated from the raw current data based on the macroscopic area of samples exposed by the mask. For AgPt@C NPs on AAO modified with silanes, EIS and chronoamperometry measurements were performed additionally. EIS was performed with a 10 mV amplitude from 100 kHz to 1 Hz at +0.45 V. Chronoamperometry was performed during 1 h at +0.45 V.

3. Results and discussions

3.1. Laser-induced deposition of AgPt@C NPs and sample characterization

In the following, at first was characterized the material obtained by LID on planar substrates glass slides coated with indium tin oxide (ITO, a classical transparent conductor). The methods will be generalized to the three-dimensional system in a subsequent step.

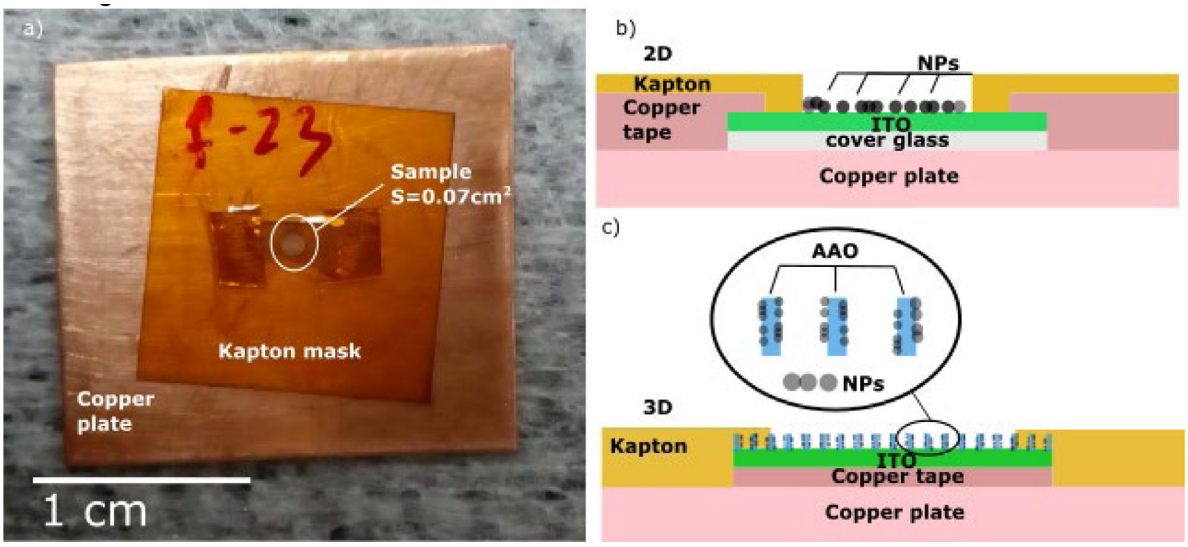

Scheme 2. Construction of electrodes from samples obtained in LID process: (**a**) macroscopic photo; (**b**) construction of electrode based on 2D sample; (**c**) construction of electrode based on 3D samples.

The laser-induced deposition is carried out from a solution of organometallic precursor $Ag_2Pt_4(CCPh)_8$, in acetophenone. LID was performed under continuous wave laser irradiation with wavelength $\lambda = 405$ nm, that is, within the absorption band of the precursor as shown in Fig. 1a. At the optimized experimental conditions (laser wavelength and power density, exposure duration, solution composition), this process leads to the formation of a hybrid material containing approximately spherical NPs in the zone of laser irradiation on the planar (2D) solid substrate surface, as demonstrated by scanning electron microscopy (SEM, Fig. 1b).

A quantitative analysis of the micrographs yields a maximum of the NPs diameter distribution function at 56 nm approximately. These particles, however, exhibit a phase-separated inner structure as observed by transmission electron microscopy in high-angle annular dark-field imaging mode (HAADF-TEM) and energy-dispersive X-ray (EDX) spectroscopic analysis (Fig. 2). The data show the presence of both metals (silver and platinum) as small inclusions embedded within a carbonaceous phase. The metal inclusions have a narrow size distribution, with an average diameter just below 2 nm.

To determine the nature of metal clusters embedded in carbonaceous phase (whether they are mono- or bimetallic), two indirect techniques were used: optical absorption spectroscopy and electrochemical characterization.

The position of plasmon resonance peaks in the absorption spectra of metal clusters depends sensitively on their composition, shape and size, so that it can be used as a diagnostic tool for distinguishing real bimetallic alloys from mechanical mixtures of monometallic clusters [54]. In particular, spherical metal clusters with a diameter below 10 nm yield a plasmon peak the position of which depends mainly on the metal nature. For pure silver and pure platinum NPs, the peak lies at 420 nm and 220 nm, respectively (with some variability depending on the dielectric constant of the matrix) [55]. Fig. 3a presents the absorption spectrum of our LID-derived material. It features two pronounced peaks, which may be assigned to two distinct types of metal clusters [56,57]. The peak at 430 nm is related to pure silver clusters. Its slight red-shift might result from the carbonaceous matrix. The peak at 350 nm is situated between the values expected for pure Pt and pure Ag particles, which therefore hints at the presence of a bimetallic phase.

Further confirmation of the presence of bimetallic AgPt particles is offered by the electrochemical properties of the material in mildly acidic aqueous solution. Electrocatalysis of the hydrogen evolution reaction (HER) is a hallmark of platinum-containing particles with small diameters [50]. The cyclic voltammetry wave presented on Fig. 3b exhibits a strong cathodic catalytic current below −0,3 V. This current, which is absent for the bare ITO substrate and starts at the thermodynamic equilibrium potential of the H^+/H_2 couple at pH = 4, can be confidently assigned to hydrogen evolution, and therefore proves the presence of Pt. However, the absence of the standard peaks associated with adsorption and desorption of atomic hydrogen on platinum (expected at slightly less negative potentials) indicates the absence of pure Pt, and thereby, the exclusively bimetallic nature of Pt-containing metal clusters. The oxidation and reduction waves at +0.4 V and +0.2 V, respectively, correspond to the oxidation of metallic silver to AgCl and its reverse reduction to Ag, respectively.

Thus, the parameters of laser-induced deposition defined for 2D substrates are transferred to the LID of AgPt@C on nanostructured (3D) anodized aluminum oxide templates. The results of depositions on as-prepared alumina substrates and on their counterparts functionalized with 3-amino-propyl-triethoxy-silane are presented in Fig. 4. Clearly, the hydrophilic oxide surface is inadequate for a proper interaction with the apolar precursor solution, so that LID results in a meager deposition on and near the top surface of as-anodized samples (Fig. 4b). Silanization yields a strongly contrasting situation, with large amounts of material deposited on the pore walls along their whole length (Fig. 4c–e, Figure S1 in the Supplementary Information). The EDX analysis from top of 3D sample shows that the composition of NPs is the same in 3D and 2D case (Figure S2 in Supplementary Information). Element analysis in depth profiles performed by EDX for silver as most intensive signal recorded from NPs, indicate that the metal loading is not perfectly constant along the pore depth. However the continuous surface decoration was observed throughout the depth even for deep (14 μm) pores.

Thus, with appropriate preliminary surface treatments, the method of laser-induced deposition allows one to obtain composite AgPt@C structures both on planar surfaces and 3D AAO substrates. In these composite electrodes, the electrocatalytic activity is provided by the metallic clusters, whereas the carbon phase (in which metal is embedded) and the underlying ITO layer provide the sample's conductivity.

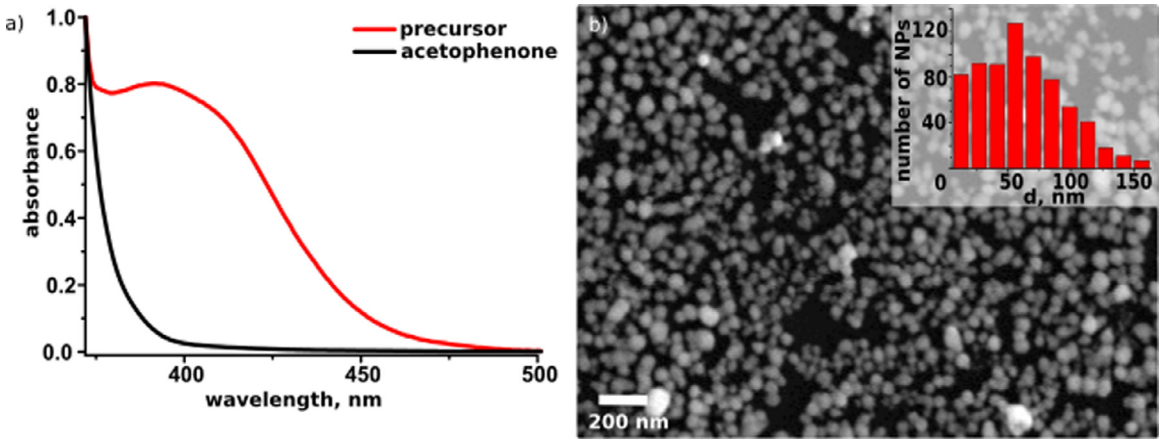

Fig. 1. (**a**) Absorbance spectra of acetophenone and the $Pt_2Ag_4(C_2Ph)_8$ precursor solution: at the laser irradiation wavelength (405 nm), only the organometallic precursor absorbs; (**b**) Scanning electron micrograph of AgPt@C deposit obtained by laser-induced deposition on ITO films; inset: NPs size distribution.

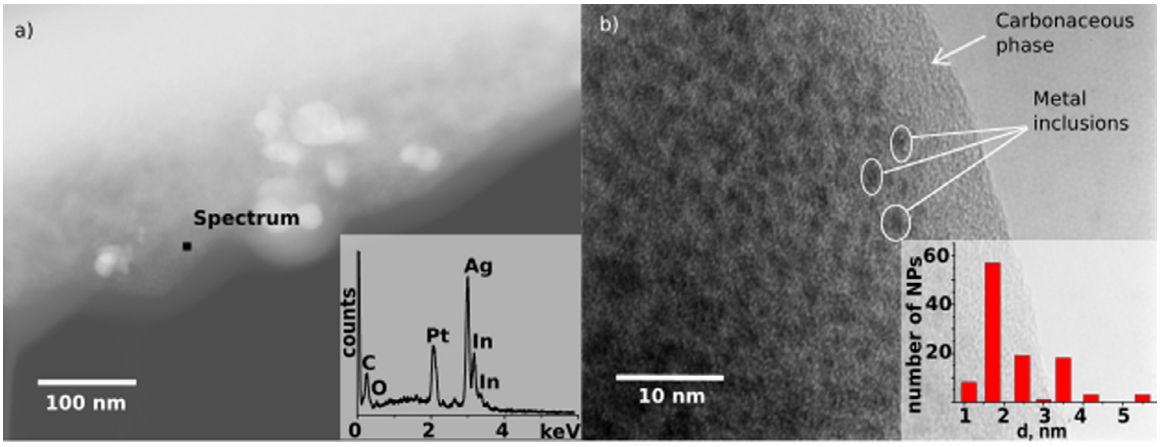

Fig. 2. Characterization of laser-deposited NPs: (**a**) HAADF TEM image of NPs in the carbonaceous matrix; on inset, EDX analysis; (**b**) bright-field TEM image of deposited NPs; on inset, size distribution of metal clusters incorporated in carbonaceous phase.

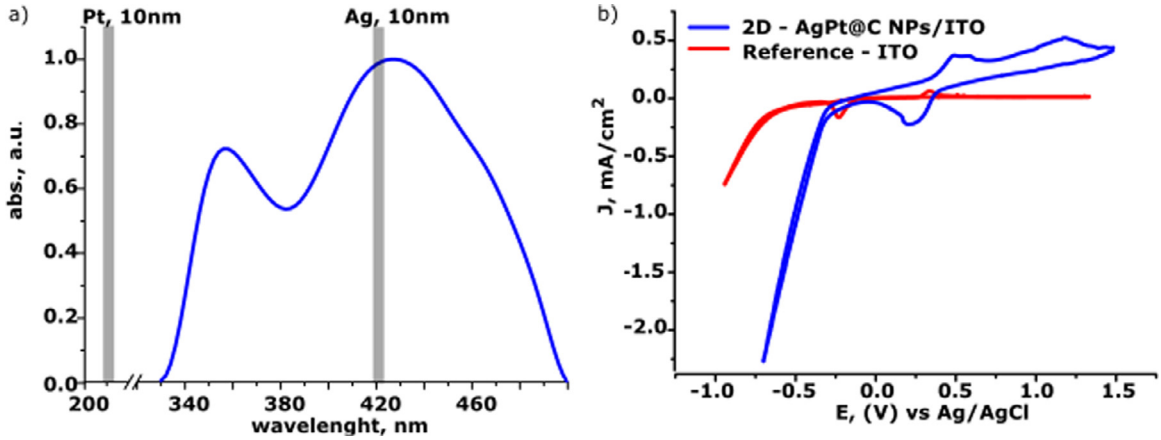

Fig. 3. Confirmation of bimetallic nature of NPs: (**a**) absorbance spectrum of the deposited NPs; gray insets define the known plasmon peak positions for monometallic Pt and Ag NPs; (**b**) cyclic voltammograms of planar AgPt@C electrodes measured in a pH 4 HCl electrolyte versus the $Ag/AgCl/KCl_{sat}$ reference electrode, and of a reference sample without NPs.

3.2. Electrocatalysis of glucose oxidation

When 5 mM of glucose are added to the mildly acidic electrolyte (pH = 4), the 2D samples (AgPt@C on ITO/glass) yield some oxidation and reduction peaks upon voltammetric cycling, which are absent from the waves recorded in absence of glucose (Fig. 5a).

As displayed on Fig. 5a, planar samples exhibit low currents, but in the presence of glucose an anodic peak appears between +0,3 V and +0,45 V. At the next step samples with 3D nanostructured geometry were investigated. The CV for sample based

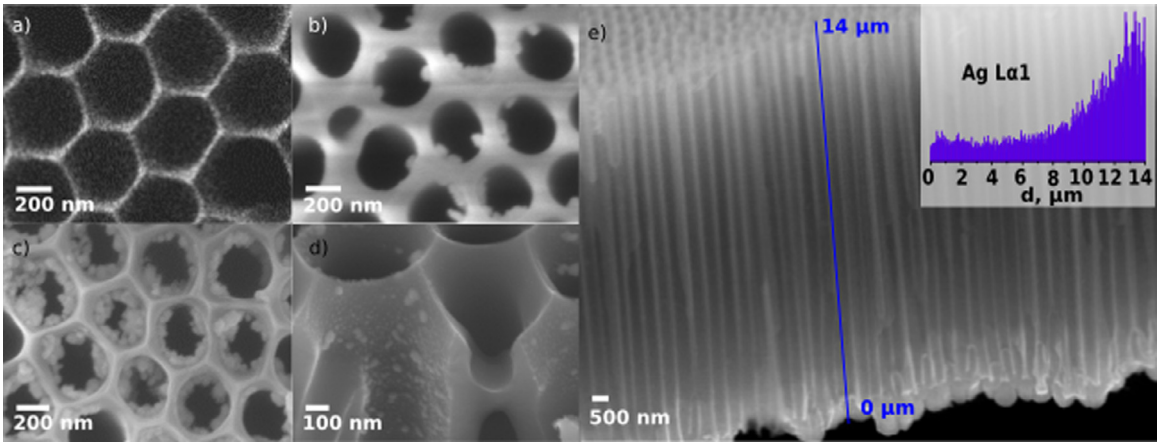

Fig. 4. Laser-induced deposition on 3D templates: (**a**) pure AAO template; (**b**) PtAg@C NPs on AAO; (**c**) PtAg@C NPs on AAO modified with silanization; (**d**) PtAg@C NPs on AAO modified with silanization — cross-section view; (**e**) silver distribution on sample, inset — EDX data across the line.

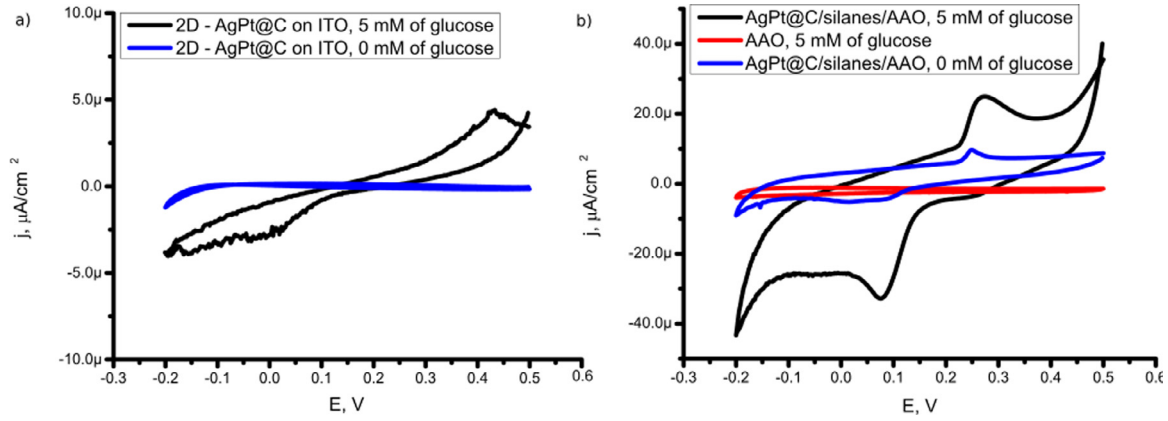

Fig. 5. Electrocatalysis of glucose oxidation on samples with various geometries. (**a**) Cyclic voltammograms (CV, 3rd cycle) recorded on 2D sample — AgPt@C NPs on ITO in presence of 5 mM of glucose and in absence of glucose (reference measurement); (**b**) glucose electrooxidation on 3D samples: CV (3rd cycle) recorded on AgPt@C NPs deposited on AAO modified with silanes; reference measurements without glucose/ without NPs are presented. All measurements were carried out vs. the $Ag/AgCl/KCl_{sat}$ reference electrode in HCl (pH = 4).. (For interpretation of the references to color in this figure legend, the reader is referred to the web version of this article.)

on non-modified AAO support in presence and absence of glucose are identical (see Figure S3 in Supplementary information) and have no catalytic currents neither any peaks, which is in agreement with SEM data and demonstrates poor deposition of NPs. The situation is completely changing in case of AgPt@C NPs on AAO support modified with silanes. Fig. 5b demonstrates a set of waves: CV for sample with AgPt@C NPs on AAO support modified with silanes in presence of 5 mM of glucose (black line) and two control measurements in absence of glucose (blue line) as well as in absence of AgPt@C NPs (red line). In contrast with 2D system, in 3D case there are oxidation and reduction peaks visible at CV in absence of glucose. The peaks at +0,05 V and +0,25 V may be related to oxidation and reduction processes taking place with the Ag of the NPs themselves, the slope in range from −0.2 V to −0.1 V may be caused by start of hydrogen evolution reaction. The full 3D surface is covered with active electrocatalyst, and with adding of glucose, current density is correspondingly much higher than in the 2D case, as expected: it reaches 25 $\mu A/cm^2$ for the oxidation of glucose to gluconolactone near +0.45 V. This current is fully caused by glucose oxidation, as proven by control experiments comparing waves recorded in the presence and absence of glucose (compare black and blue lines on Fig. 5b). The shift for peaks related to processes on NPs may be caused by higher involving of bimetallic clusters in surface reaction. The voltammetric waves on Fig. 5 has a shape similar to those obtained on Ag in basic medium [58–60], but is shifted according to expectations based on pH.

To investigate the stability of AgPt@C/silanes/AAO samples chronoamperometry measurements were performed. Fig. 6a demonstrates that during chronoamperometry measurements at +0.45 V, the sample demonstrates stable current. The CVs for the sample before and after chronoamperometry measurements are presented in Supplementary Information, Figure S4.

To obtain information about the kinetics of the reaction, impedance spectroscopy for AgPt@C/silanes/AAO sample was performed (Fig. 6b). The response of the sample is an almost straight line, which is typical for systems in which transport plays the most important role [61]. The equivalent circuit model is presented on Fig. 6b, fitted curve is in solid line. Value of the most important element — charge-transfer resistance (R_{ct}) at the electrolyte/electrode interface is 628 kΩ.

4. Conclusions

In this article, hybrid AgPt@C nanoparticles were prepared for the first time with laser-induced deposition; bimetal supramolecular complex $Pt_2Ag_4(C_2Ph)_8$ was used as the organometallic precursor. The deposited nanostructures were found to be carbon nanoparticles ca 56 nm in diameter with bimetal Ag–Pt nanoinclusions ca 2 nm. The procedure of AgPt@C NPs formation was

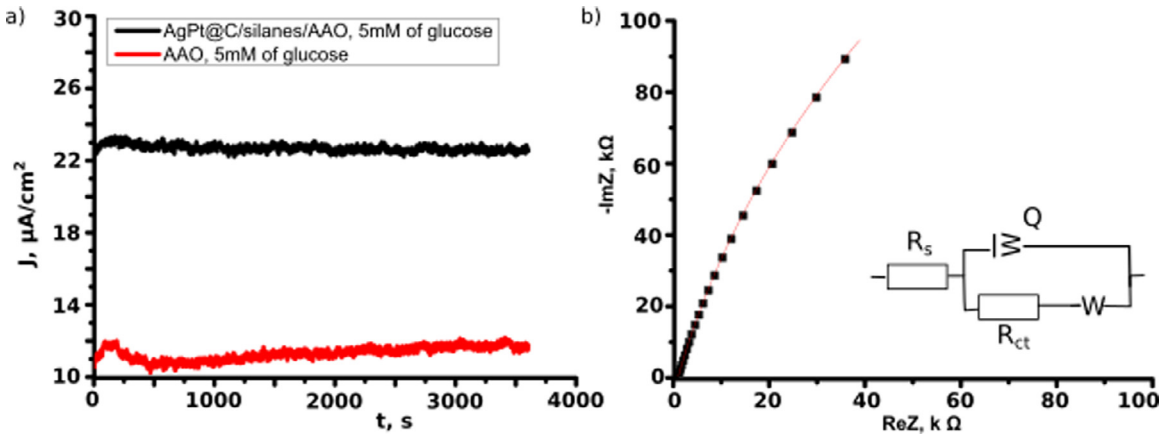

Fig. 6. (**a**) chronoamperometry measurements for AgPt@C/silanes/AAO sample; (**b**) impedance spectroscopy of AgPt@C/silanes/AAO sample.

successfully demonstrated for both 2D and 3D substrates. As 3D substrates the AAO templates were used. In spite of high AAO aspect ratio (pore length to diameter ca 100:1), continues pore decoration with NPs was demonstrated. It was found that a preliminary silanization of the anodic aluminum oxide surface favors more homogeneous AgPt@C NPs formation. Obtained samples are applicable to non-enzymatic electrocatalysis of glucose oxidation in mildly acidic medium. The performance of these AgPt@C NPs/AAO electrodes can be tuned based on the geometric parameters of the AAO substrate.

Funding

This work was supported by RFBR-DFG (RFBR project №20 — 58 — 12015, DFG project BA 4277/16 — 1); (laser-induced deposition and characterization parts), RFBR project (Russian Federation) №19 — 33 — 90239 (electrochemical part), by the "Scholarships of the President of the Russian Federation to young scientists and graduate students (Competition SP-2019) (Russian Federation)", project number СП-2368.2019.1 and by Saint-Petersburg State University (Russian Federation) (project ID 41128217).

CRediT authorship contribution statement

Anna Vasileva: Investigation, Data curation, Writing - original draft, Visualization, Funding acquisition. **Sandra Haschke:** Investigation, Writing - review & editing. **Vladimir Mikhailovskii:** Investigation, Data curation,. **Anastasia Gitlina:** Investigation, Writing - original draft, . **Julien Bachmann:** Conceptualization, Writing - original draft, Writing - review & editing, Supervision, Funding acquisition. **Alina Manshina:** Conceptualization, Methodology, Writing - original draft, Writing - review & editing, Supervision, Project administration, Funding acquisition.

Declaration of competing interest

The authors declare that they have no known competing financial interests or personal relationships that could have appeared to influence the work reported in this paper.

Acknowledgments

Authors are grateful to "Centre for Optical and Laser materials research", "Centre for X-ray Diffraction Studies" and "Interdisciplinary Resource Centre for Nanotechnology" of Research Park of Saint Petersburg State University for technical support.

Appendix A. Supplementary data

Supplementary material related to this article can be found online at https://doi.org/10.1016/j.nanoso.2020.100547.

References

[1] D. Riman, K. Spyrou, A.E. Karantzalis, J. Hrbac, Glucose sensing on graphite screen-printed electrode modified by sparking of copper nickel alloys, Talanta 165 (2017) 466–473.
[2] L. Mei, P. Zhang, J. Chen, D. Chen, Y. Quan, Non-enzymatic sensing of glucose and hydrogen peroxide using a glassy carbon electrode modified with a nanocomposite consisting of nanoporous copper, carbon black and nafion, Microchim. Acta 183 (2016) 1359–1365.
[3] X. Niu, H. Zhao, M. Lan, L. Zhou, Platinum nanoparticles encapsulated in carbon microspheres: Toward electro-catalyzing glucose with high activity and stability, Electrochim. Acta 151 (2015) 326–331.
[4] Z. Gao, J. Guo, N. Shrestha, R. Hahn, Y. Song, P. Schmuki, Nickel hydroxide nanoparticle activated semi-metallic TiO_2 nanotube arrays for non-enzymatic glucose sensing, Chem. Eur. J. 19 (2013) 15530–15534.
[5] V. Coyle, A. Kandjani, Y. Sabri, S. Bhargava, Au nanospikes as a non-enzymatic glucose sensor: Exploring morphological changes with the elaborated chronoamperometric method, Electroanalysis 29 (2017) 294–304.
[6] S. Felix, P. Kollu, S. Jeong, A. Grace, A novel CuO–N-doped graphene nanocomposite-based hybrid electrode for the electrochemical detection of glucose, Appl. Phys. A 123 (2017) 620.
[7] A. Heller, Feldman. B., Electrochemistry in diabetes management, Acc. Chem. Res. 43 (7) (2010) 963–973.
[8] A. Saei, J. Dolatabadi, P. Najafi-Marandi, A. Abhari, M. Guardia, Electrochemical biosensors for glucose based on metal nanoparticles, TRAC Trends Anal. Chem. 42 (2013) 216–227.
[9] S. Barman, M. Hossain, J. Park, Soft surfactant-assisted uniformly dispersed platinum nanoparticles for high performance electrochemical non-enzymatic glucose sensing platform, J. Electroanal. Chem. 824 (2018) 121–127.
[10] H. Karimi-Maleh, F. Karimi, M. Alizadeh, A.L. Sanati, Electrochemical sensors, a bright future in the fabrication of portable kits in analytical systems, Chem. Rec. 20 (2020) 682–692.
[11] A.M. M. Jani, D. Losic, N.H. Voelcker, Nanoporous anodic aluminium oxide: Advances in surface engineering and emerging applications, Prog. Mater. Sci. 58 (2013) 636–704.
[12] A. Santos, P. Formentín, J. Pallarès, L.F. Marsal, Nanoporous anodic alumina obtained without protective oxide layer by hard anodization, Mater. Lett. 67 (2012) 296–299.
[13] H. Kynclová, J. Smilek, P. Sedláček, J. Prášek, M. Klučáková, J. Hubálek, Preparation and utilization of alumina oxide membranes for sensor devices, Mater. Sci. Forum 851 (2016) 159–164.
[14] L. Assaud, S. Bochmann, S. Christiansen, J. Bachmann, A large electrochemical setup for the anodization of aluminum towards highly ordered arrays of cylindrical nanopores, Rev. Sci. Instrum. (2015) 73902.
[15] S.M. Suchitra, P.R. Reddy, N.K. Udayashankar, Effect of pore widening time on the structural aspects of self- organized nanopore arrays formed by anodization of aluminum in chromic acid, Mater. Today Proc. 3 (2016) 2042–2051.

[16] M. Michalska-Domańska, M. Norek, W.J. Stępniowski, B. Budner, Fabrication of high quality anodic aluminum oxide (AAO) on low purity aluminum—A comparative study with the AAO produced on high purity aluminum, Electrochim. Acta 105 (2013) 424–432.
[17] M. Michalska-Domańska, W.J. Stępniowski, M. Salerno, Effect of inter-electrode separation in the fabrication of nanoporous alumina by anodization, J. Electroanal. Chem 823 (2018) 47–53.
[18] T. Tatsuya Kikuchi, O. Nishinaga, S. Natsui, R.O. Suzuki, Fabrication of self-ordered porous alumina via etidronic acid anodizing and structural color generation from submicrometer-scale dimple array, Electrochim. Acta 156 (2015) 235–243.
[19] C. Zhang, Y. Zhang, X. Du, Y. Chen, W. Dong, B. Han, Q. Chen, Facile fabrication of Pt-Ag bimetallic nanoparticles decorated reduced graphene oxide for highly sensitive non-enzymatic hydrogen peroxide sensing, Talanta 159 (2016) 280–286.
[20] X. Cao, N. Wang, Y. Han, C. Gao, Y. Xu, M. Li, Y. Shao, PtAg bimetallic nanowires: Facile synthesis and their use as excellent electrocatalysts toward low-cost fuel cells, Nano Energy 12 (2015) 105–114.
[21] N. Long, Y. Yang, C. Thi, N. Minh, Y. Cao, M. Nogami, The development of mixture, alloy, and core-shell nanocatalysts with nanomaterial supports for energy conversion in low-temperature fuel cells, Nano Energy 5 (2013) 636–676.
[22] Z. Li, Y. Li, C. He, P. Shen, Bimetallic PtAg alloyed nanoparticles and 3D mesoporous graphene nanosheet hybrid architectures for advanced oxygen reduction reaction electrocatalysts, J. Mater. Chem. A 5 (2017) 23158–23169.
[23] R. Nazir, P. Fageria, M. Basu, S. Pande, Decoration of carbon nitride surface with bimetallic nanoparticles (Ag/Pt, Ag/Pd, and Ag/Au) via galvanic exchange for hydrogen evolution reaction, J. Phys. Chem. C 121 (36) (2017) 19548–19558.
[24] D. Ma, X. Tang, M. Guo, H. Lu, X. Xu, Fabrication and characterization of non-enzymatic glucose sensor based on bimetallic hollow Ag/Pt nanoparticles prepared by galvanic replacement reaction, Ionics 21 (2015) 1417–1426.
[25] H. Kazici, M. Yayla, An electrocatalyst for detection of glucose in human blood: Synergy in Pd–AuNPs/GOx/C surfaces, J. Chem. Engin. Com. 206 (2019) 1731–1742.
[26] S. Haschke, D. Pankin, V. Mikhailovskii, M.K.S. Barr, A. Both-Engel, A. Manshina, J. Bachmann, Nanoporous water oxidation electrodes with a low loading of laser-deposited Ru/C exhibit enhanced corrosion stability, Beilstein J. Nanotechnol. 10 (2019) 157–167.
[27] A. Manshina, A. Povolotskiy, T. Ivanova, A. Kurochkin, Y. Tver'yanovich, D. Kim, M. Kim, S. Kwon, Laser-assisted metal deposition from $CuSO_4$ - based electrolyte solution laser, Phys. Lett. Arch. 4 (2007) 163–167.
[28] A.C. Lamont, A.T. Alsharhan, R.D. Sochol, Geometric determinants of in-situ direct laser writing, Sci. Rep. 9 (2019) 394.
[29] P. Nancy, J. James, S. Valluvadasan, R.A.V. Kumar, Laser – plasma driven green synthesis of size controlled silver nanoparticles in ambient liquid, Nano-Struct. Nano-Objects 16 (2018) 337–346.
[30] A.A. Popov, G. Tselikov, N. Dumas, C. Berard, K. Metwally, N. Jones, A. Al-kattan, B. Larrat, D. Braguer, S. Mensah, A. Da Silva, M. Estève, A.V. Kabashin, Laser- synthesized TiN nanoparticles as promising plasmonic alternative for biomedical applications, Sci. Rep. 9 (2019) 1194.
[31] X. Song, K.L. Xiao, X.Q. Wu, G. Wilde, M.Q. Jiang, Nanoparticles produced by nanosecond pulse laser ablation of a metallic glass in water, J. Non-Cryst. Solids 517 (2019) 119–126.
[32] Y. Xu, L. Yan, X. Li, H. Xu, Fabrication of transition metal dichalcogenides quantum dots based on femtosecond laser ablation, Sci. Rep. 9 (2019) 2931.
[33] A.A. Vasileva, I.A. Nazarov, P.K. Olshin, A.V. Povolotskiy, I.A. Sokolov, A.A. Manshina, Structural features of silver-doped phosphate glasses in zone of femtosecond laser-induced modification, J. Solid State Chem. 230 (2015) 56–60.
[34] N. Nedyalkov, N.E. Stankova, M.E. Koleva, R. Nikov, L. Aleksandrov, R. Iordanova, G. Atanasova, E. Iordanova, G. Yankov, Applied surface science laser processing of noble metal doped glasses by femto- and nanosecond laser pulses, Appl. Surf. Sci. 475 (2019) 479–486.
[35] A. Povolotckaia, D. Pankin, Y. Petrov, A. Vasileva, I. Kolesnikov, Plasmonic carbon nanohybrids from laser-induced deposition: Controlled synthesis and SERS properties, J. Mater. Sci. 54 (2019) 8177–8186.
[36] P. Dharmalingam, K. Venkatakrishnan, B. Tan, An atomic-defect enhanced Raman scattering (DERS) quantum probe for molecular level detection – breaking the SERS barrier, Appl. Mater. Today 16 (2019) 28–41.
[37] A.G.B. Jr, P. Cavassin, T.N. Machado, Surface-enhanced Raman scattering using bismuth nanoparticles : A study with aminoacids, J. Nanopart. Res. 19 (2017) 362.
[38] A. Vasileva, D. Pankin, I. Kolesnikov, S. Rzhevskiy, A. Manshina, Laser-deposited hybrid Au-Ag@C nanoparticles as efficient SERS & adsorption material, J. Phys. Conf. Ser. 1124 (2018) 51029.
[39] I. Olvera-Rodríguez, R. Hernández, A. Medel, C. Guzmán, Separation and purification technology TiO_2/Au/TiO_2 multilayer thin film photoanodes synthesized by pulsed laser deposition for photoelectrochemical degradation of organic pollutants, Sep. Purif. Technol. 224 (2019) 189–198.
[40] C. Bak, H. Wook, C. Lee, D. Jeong, H. Eom, Laser irradiation synthesis and photocatalytic properties of TiO_2-SiO_2 hybrid thin films, Thin Solid Film. J. 678 (2019) 32–41.
[41] S. Schlicht, A. Kireev, A. Vasileva, E.V. Grachova, A model electrode of well-de fi ned geometry prepared by direct laser-induced decoration of nanoporous templates with AuAg@C nanoparticles, Nanotechnology 28 (2017) 65405.
[42] Y. Wang, A. Tabetoul, M. Mohamedi, Laser synthesis of hierarchically organized nanostructured TiO_2 films on micro fibrous carbon paper substrate: Characterization and electrocatalyst supporting properties, J. Power Sources 299 (2015) 149–155.
[43] K. Zhang, S.K. Maurya, R.A. Ganeev, Ablated nickel nanoparticles: Third harmonic generation and optical nonlinearities, J. Opt. 20 (2018) 125502.
[44] J. Guay, A.C. Lesina, G. Killaire, P.G. Gordon, C. Hahn, S.T. Barry, L. Ramunno, P. Berini, A. Weck, Laser-written colours on silver: Optical effect of alumina coating, Nanophotonics 8 (2019) 807–822.
[45] M.A. Butt, A.C. Lesina, M. Neugebauer, T. Bauer, L. Ramunno, A. Vaccari, P. Berini, Y. Petrov, D. Danilov, A. Manshina, P. Banzer, G. Leuchs, Investigating the optical properties of a laser induced 3D self-assembled carbon – metal hybrid structure, Small 15 (2019) 1900512.
[46] M.Y. Bashouti, A.V. Povolotckaia, A.V. Povolotskiy, S.P. Tunik, S.H. Christiansen, G. Leuchs, A.A. Manshina, Spatially-controlled laser-induced decoration of 2D and 3D substrates with plasmonic nanoparticles, RSC Adv. 2 (2016) 75681–75685.
[47] A. Manshina, E. Grachova, A. Povolotskiy, A. Povolotckaia, Y. Petrov, I. Koshevoy, A. Makarova, D. Vyalikh, S.P. Tunik, Laser-induced transformation of supramolecular complexes: Approach to controlled formation of hybrid multi-yolk-shell Au-Ag@a-C:H nanostructures, Sci. Rep. 5 (2015) 12027.
[48] D. Liu, L. Li, T. You, Superior catalytic performances of platinum nanoparticles loaded nitrogen-doped graphene toward methanol oxidation and hydrogen evolution reaction, J. Colloid Interface Sci. 487 (2017) 330–335.
[49] J. Ye, Z. Liu, C. Lai, C. Lo, C. Lee, Diameter effect of electrospun carbon fiber support for the catalysis of Pt nanoparticles in glucose oxidation, Chem. Eng. J. 283 (2016) 304–312.
[50] W. Yu, M.D. Poroso, J.G. Chen, Review of Pt-based bimetallic catalysis: From model surfaces to supported catalysts, Chem. Rev. 112 (2012) 5780–5817.
[51] P. Espinet, J. Forniés, F. Martinez, M. Tomas, Polynuclear platinum–silver, –copper and –gold acetylide complexes. molecular structure of $[Pt_2Ag_4(CCBu^t)_8]$, J. Chem. Soc. Dalton Trans. (1990) 791–798.
[52] V. Sivchik, A. Solomatina, Y.-T. Chen, A. Karttunen, S.P. Tunik, P.-T. Chou, I. Koshevoy, Halogen bonding to amplify luminescence: A case study using a platinum cyclometalated complex, Angew. Chem. Int. Ed. 54 (2015) 14057–14060.
[53] W.L.F. Armarego, in: C. Chai (Ed.), Purification of Laboratory Chemicals, 6th ed., Elsevier, ISBN: 978-1-85617-567-8, 2009, p. 760.
[54] A. Rubio, Modified Au-Based Nanomaterials Studied By Surface Plasmon Resonance Spectroscopy, Springer International Publishing, 2015.
[55] M.A. Garcia, Surface plasmons in metallic nanoparticles : Fundamentals, J. Phys. D. Appl. Phys. 45 (2012) 389501.
[56] M. Mallin, C. Murphy, Solution-phase synthesis of sub-10 nm Au-Ag alloy nanoparticles, Nano Lett. 2 (11) (2002) 1235–1237.
[57] K. Kim, Kim. K., S. Lee, Surface enrichment of Ag atoms in Au/Ag alloy nanoparticles revealed by surface enhanced Raman scattering spectroscopy, Chem. Phys. Lett. 403 (1–3) (2005) 77–82.
[58] J. Xu, X. Qiao, M. Arsalan, N. Cheng, W. Cao, T. Yue, Preparation of one dimensional silver nanowire/nickel-cobalt layered double hydroxide and its electrocatalysis of glucose, J. Electroanal. Chem. 823 (2018) 315–321.
[59] M. Baghayeri, A. Amiri, S. Farhadi, Chemical development of non-enzymatic glucose sensor based on efficient loading Ag nanoparticles on functionalized carbon nanotubes, Sensors Actuators B 225 (2016) 354–362.
[60] H. Quan, S. Park, J. Park, Electrochemical oxidation of glucose on silver nanoparticle-modified composite electrodes, Electrochim. Acta 55 (2010) 2232–2237.
[61] J. Bachmann, J. Jing, M. Knez, S. Barth, H. Shen, S. Mathur, U. Gösele, K. Nielsch, Ordered iron oxide nanotube arrays of controlled geometry and tunable magnetism by atomic layer deposition, J. Am. Chem. Soc. 129 (2007) 9554–9555.